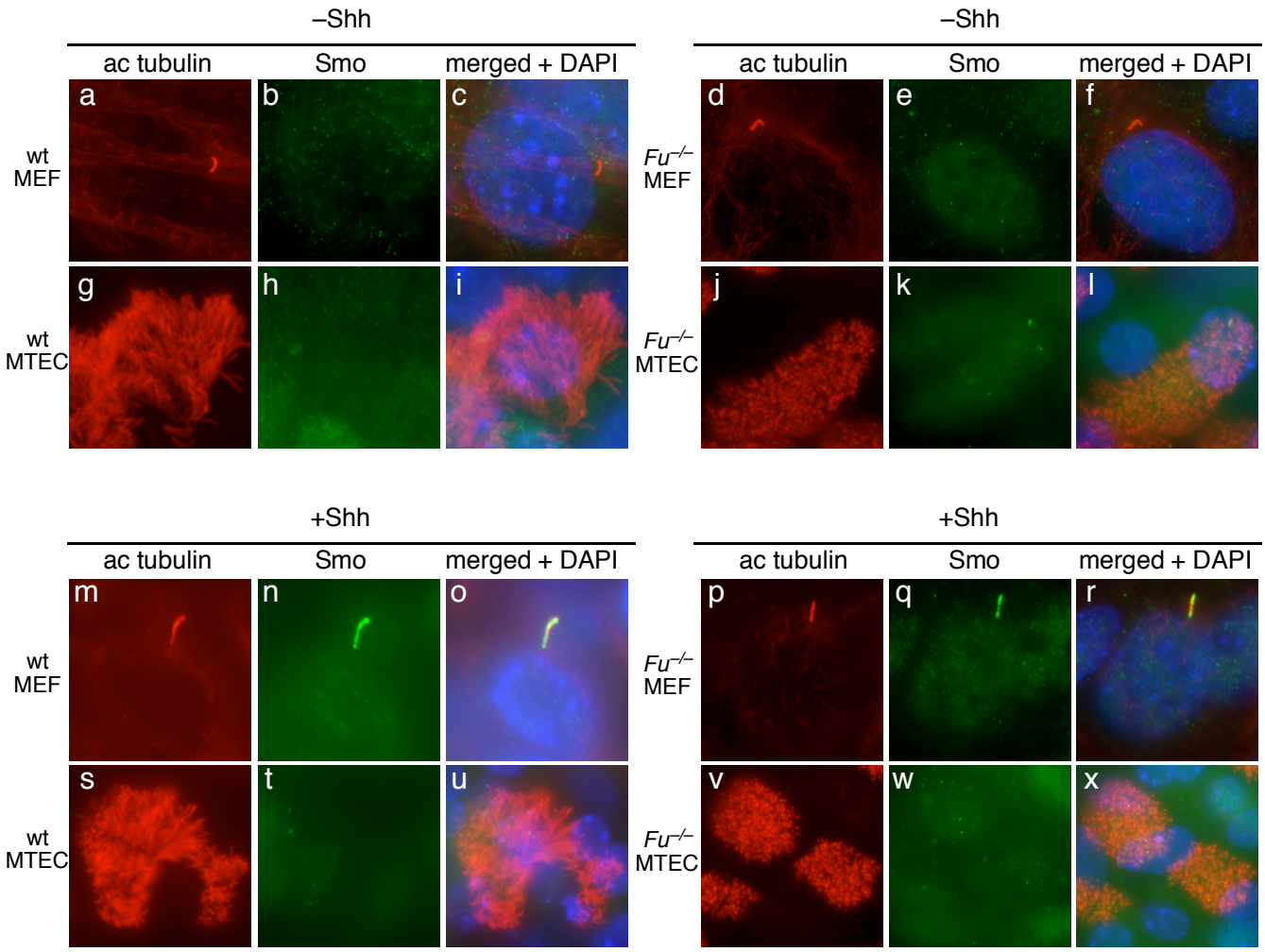

Supplementary Figure 1: *Fu*$^{-/-}$ mouse embryonic fibroblasts (MEFs), but not mouse tracheal epithelial cells (MTECs), are Hh-responsive

a-f, Immunofluorescence of acetylated tubulin (ac tubulin, red signal) and Smoothened (Smo, green signal) on primary cilia of wild-type (wt) (**a-c**) and *Fu*$^{-/-}$ (**d-f**) immortalized MEFs. MEFs were grown to confluence on gelatin-coated (Sigma) coverslips and treated with ShhN-conditioned media[38] to activate Hh signaling for 1 hr. Immunostaining was performed using standard procedures with mouse anti-acetylated tubulin (Sigma, 1:2000) and rabbit anti-Smo[39] (Chen et al, manuscript in preparation) and images were obtained on a Nikon E1000 epifluorescence microscope using a 100x oil immersion lens. Construction of primary cilia and translocation of Smo to the primary cilium in response to exogenous ShhN are unaffected in *Fu*$^{-/-}$ MEFs. **g-l**, Epifluorescence of acetylated tubulin and Smo on motile cilia of wt (**g-i**) and *Fu*$^{-/-}$ (**j-l**) MTECs. Smo is not detectable on motile cilia in either wt or *Fu*$^{-/-}$ cells treated apically with ShhN.

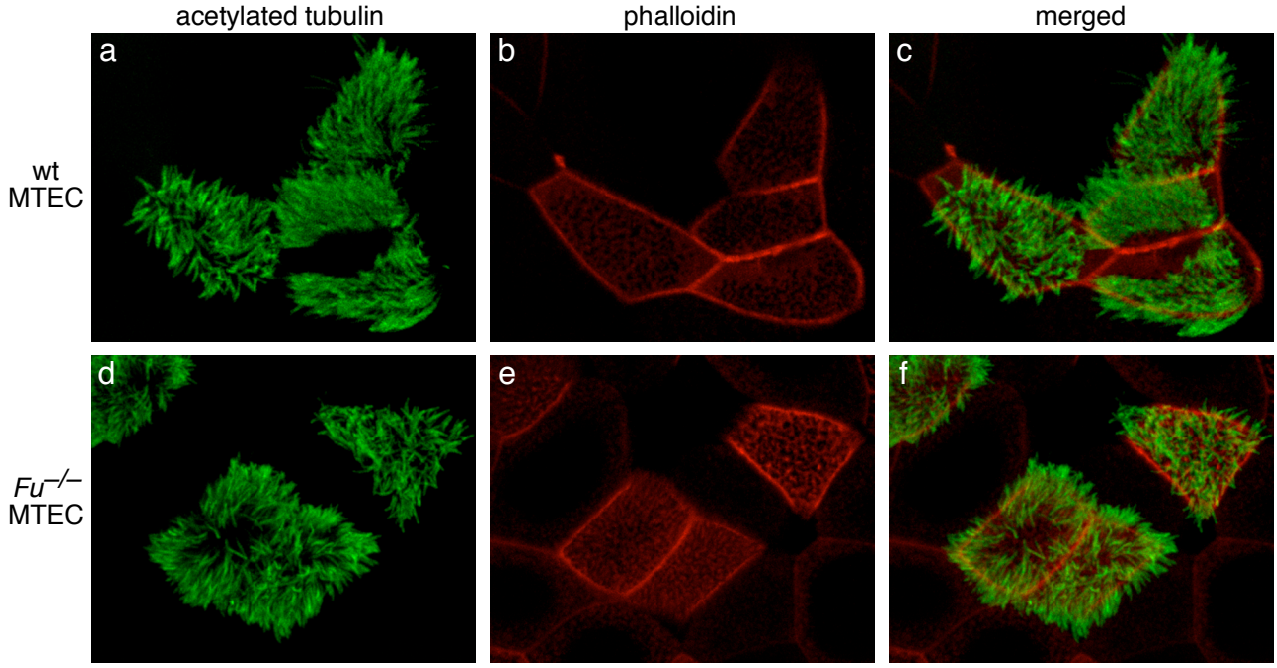

Supplementary Figure 2: The apical actin network and motile cilia outgrowth are unaffected in *Fu*$^{-/-}$ MTECs

a-f, Confocal immunofluorescence of acetylated tubulin (green) and rhodamine-phalloidin (red) in wild-type (wt) (**a-c**) and *Fu*$^{-/-}$ mouse tracheal epithelial cells (MTECs) (**d-f**). No differences in apical-basolateral polarization or cilia outgrowth were observed in the absence of *Fu*.

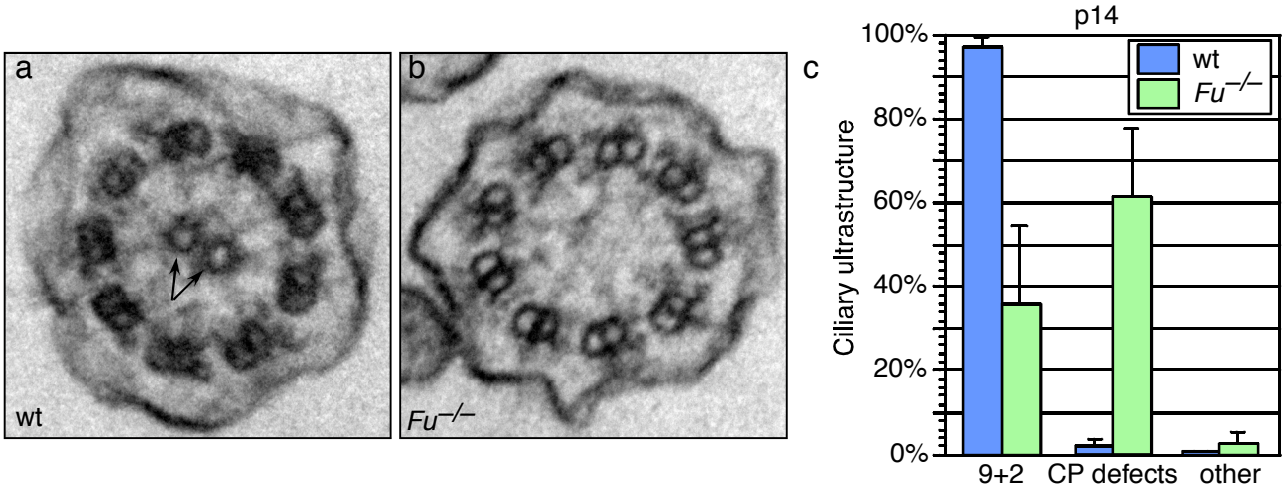

Supplementary Figure 3: Fused is required for central pair (CP) assembly in ependymal cilia **a**, **b,** Transmission electron micrographs of motile cilia from wild-type (wt) and *Fu*$^{-/-}$ mouse ependymal cells at postnatal (p) day 14. Arrows denote the CP microtubules. **c**, Quantification of ultrastructural defects from p14 ependymal cells (wt, n = 2 animals, mean 147 cilia/animal analyzed; *Fu*$^{-/-}$, n = 2, mean 61 cilia/animal analyzed). Error bars indicate standard deviation (s.d.). In a subset of ependymal or tracheal axonemes that lack the CP, outer doublet translocations, in which an outer doublet MT pair moves to the position occupied by the CP, were also observed (data not shown). *Fu*-deficient mice do not display organ laterality defects (data not shown), indicating normal function of the mouse node, which establishes left-right asymmetry during embryogenesis. *Fu*$^{-/-}$ mice developed respiratory infections, highly penetrant hydrocephalus, stunted growth and poor general health that likely led to lethality (data not shown)[6,7].

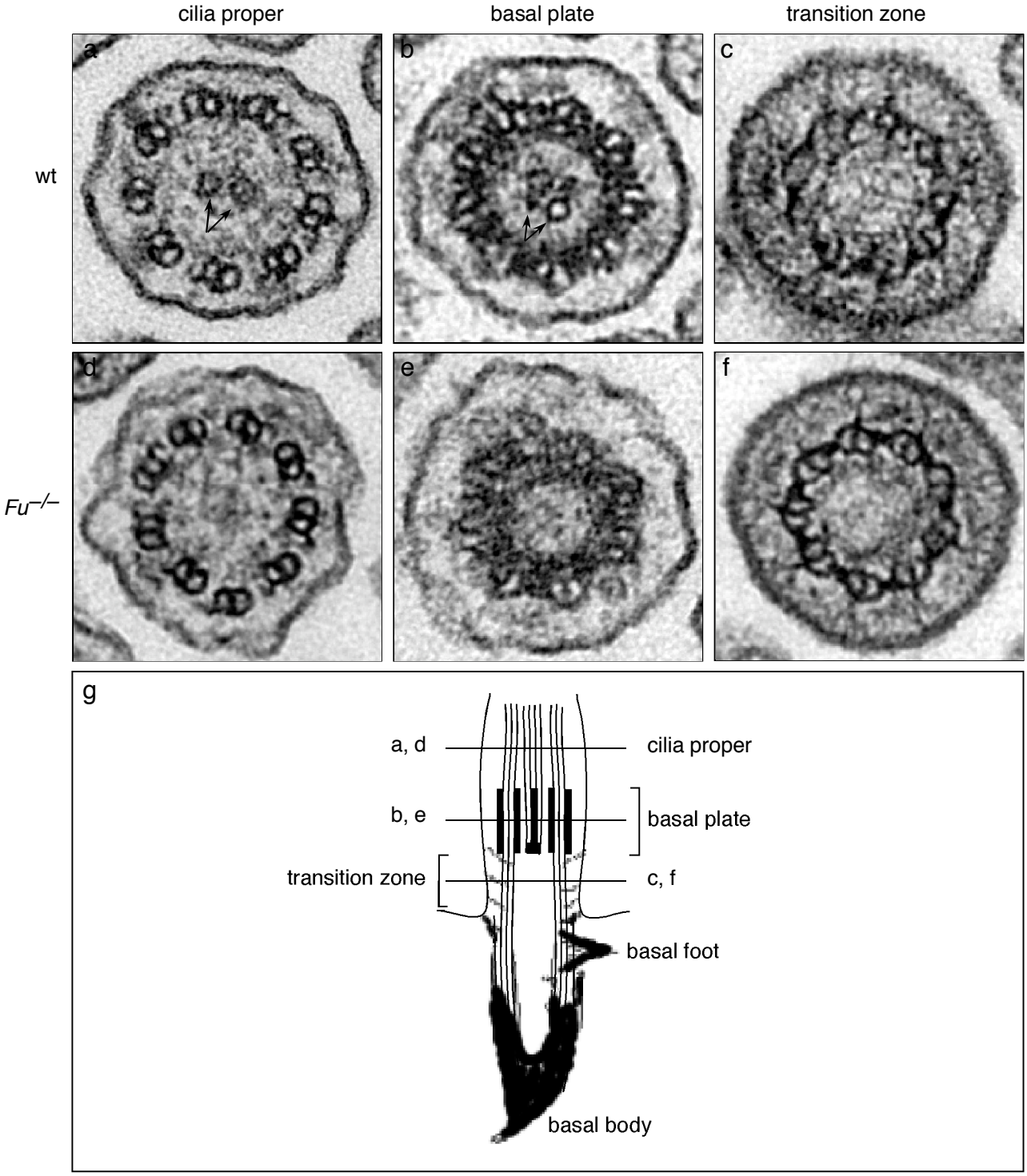

Supplementary Figure 4: Central pair defects in *Fu*$^{-/-}$ animals originate at the basal plate
a-f, Transmission electron micrographs of motile cilia axonemes from wild-type (wt) and *Fu*$^{-/-}$ tracheae. Arrows denote the CP microtubules. In *Fu*$^{-/-}$ animals, CP microtubules are missing in both the axonemes (**d**) and in the basal plate (**e**), which is characterized by electron dense material surrounding the outer microtubules and is the site of CP outgrowth[14]. Outer microtubule doublets and associated structures are grossly normal in *Fu*$^{-/-}$ animals (**f**). **g**, Schematic lateral view of a wt 9+2 cilium depicting the locations of the transition zone, basal plate, and ciliary axoneme.

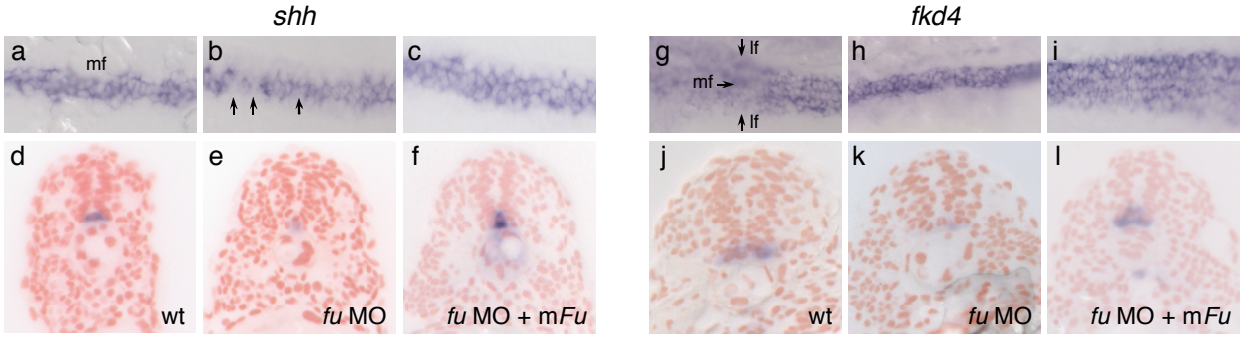

Supplementary Figure 5: Mouse *Fu* rescues lateral floor plate in zebrafish *fu* morphants
a-c, Whole-mount *in situ* hybridization to *shh* (purple signal) in the medial floor plate of wt, *fu* morphants, and *fu* morphants expressing mouse *Fu* at 24 hours post fertilization (hpf). View is dorsal. Reduced *shh* expression in *fu* morphants (**b**) (arrows) is consistent with an inability to maintain medial floor plate in the absence of *fu*; *shh* expression in *fu* morphants is restored to wt levels when mouse *Fu* is expressed (**c**). mf, medial floor plate. **d-f**, Cross section of embryos shown in **a-c** at the trunk region. **g**, Whole-mount *in situ* hybridization to *fkd4* (purple signal) in both medial and lateral floor plates of wt zebrafish embryos at 24 hpf. View is dorsal. **h**, **i**, *fkd4* expression is lost in the lateral floor plate of *fu* morphants (**h**) and is restored when mouse *Fu* is expressed (**i**). mf, medial floor plate; lf, lateral floor plate. **g-i** are zoomed-out images of panels in **Fig. 2a-c**. **j-l**, Cross section of embryos shown in **g-i** at the trunk region.

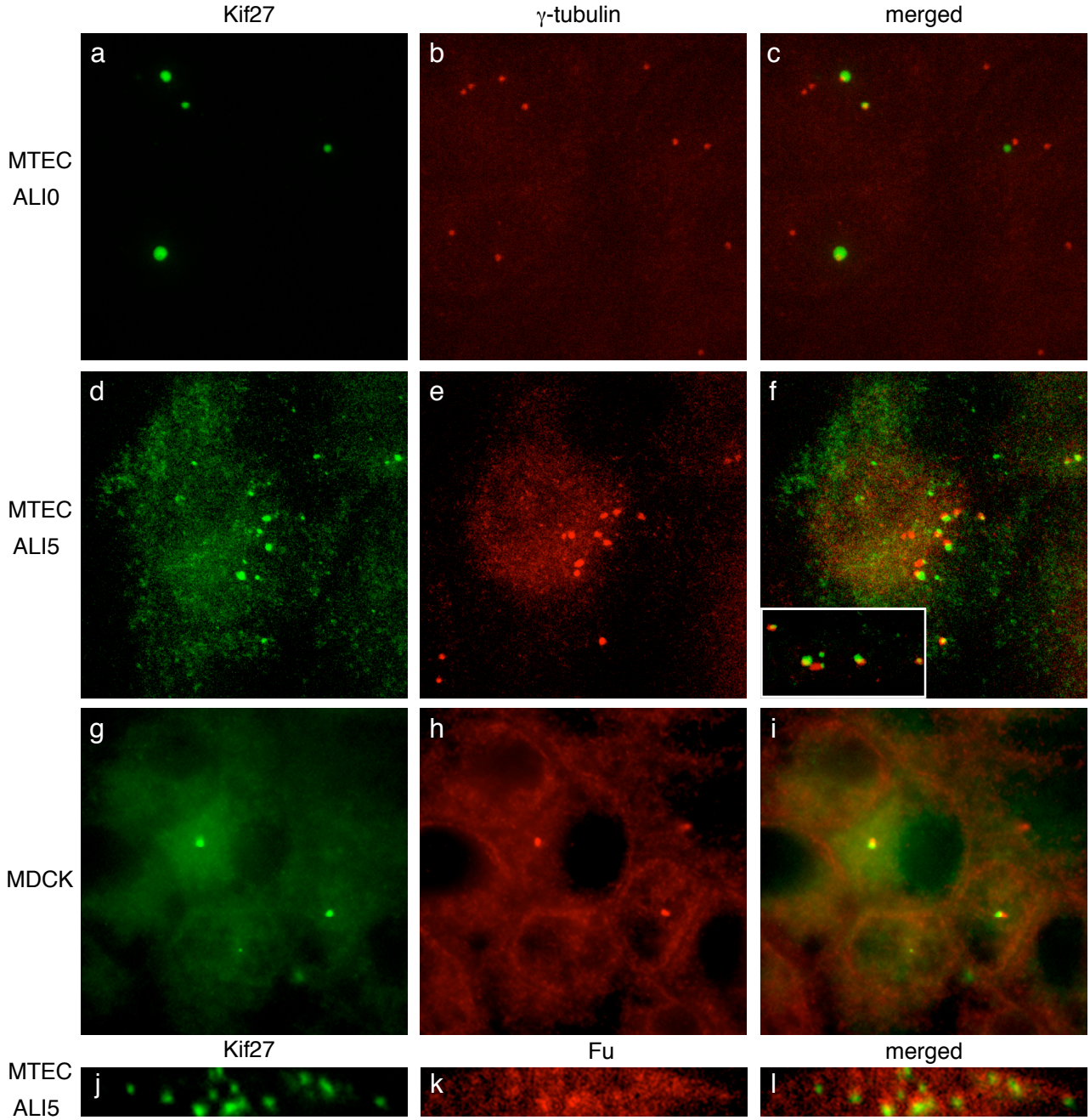

Supplementary Figure 6: Kif27 localizes to centrioles and basal bodies in MTECs and polarized MDCK cells while Fu is broadly expressed in the cytoplasm

a-f, Confocal immunofluorescence of lentivirally transduced Kif27-GFP and mouse anti-γ-tubulin (red) (Sigma, 1:1000) in mouse tracheal epithelial cells (MTECs) at air-liquid interface (ALI) days 0 (**a-c**) and 5 (**d-f**). Kif27-GFP remains associated with centrioles throughout ciliogenesis. The inset in (**f**) is a 3-dimensional reconstruction of the confocal stack in (**f**) using the VolumeViewer plugin in NIH ImageJ. **g-i**, Kif27-GFP localizes to apical basal bodies (assessed by epifluorescence) in polarized Madin-Darby canine kidney (MDCK) cells. MDCK cells were maintained in MEM Eagle's with Earle's balanced salt solution (Cellgro) supplemented with 5% fetal bovine serum (Gibco) and grown on gelatin-coated glass coverslips. Kif27 in pEGFP-N1 was transfected using Lipofectamine 2000 (Invitrogen) according to manufacturer's instructions. **j-l**, Confocal immunofluorescence (xz projections) of lentivirally transduced Kif27-GFP and Fu-mCherry (red) in MTECs at ALI day 5. Fu-mCherry is broadly expressed in the cytoplasm and overlaps with Kif27-GFP expression. Similar expression patterns were observed in MDCKs and MEFs (data not shown). We have also examined localization of Kif27-GFP in *Fu*$^{-/-}$ MTECs and found that its localization to the base of the cilium is not drastically perturbed (data not shown).

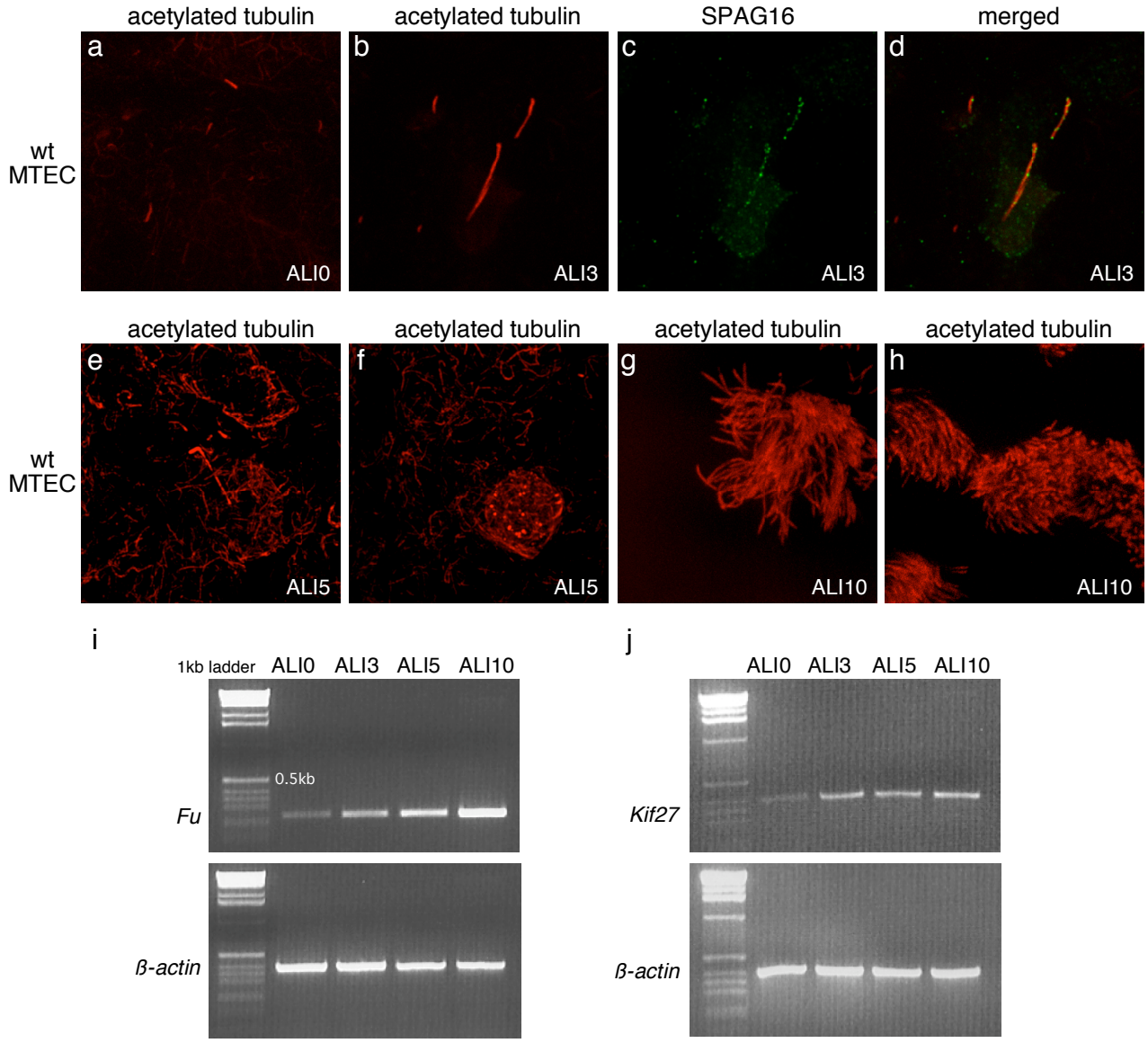

Supplementary Figure 7: Conversion of primary cilia to motile cilia is accompanied by upregulation of *Fu* and *Kif27* expression during MTEC differentiation

a-h, Confocal immunofluorescence of acetylated tubulin (red) and Spag16L (green) in wild-type MTECs at air-liquid interface (ALI) days 0, 3, 5 and 10. As previously reported[37], MTECs display short cilia at their apical surface prior to creation of ALI (**a**). Long cilia are observed a few days after differentiation is induced (**b**); these cilia display punctae of SPAG16L[26], a central pair protein, along the length of the axoneme (**c**, **d**). Persistence of these long cilia was observed up to ALI5 (**e**). After this point, microtubules accumulated at the apical surface of the MTECs, and outgrowth of motile cilia axonemes was initiated (**e-h**). These axonemes also exhibited Spag16L punctae (data not shown). Further, Spag6 and Spag16L localization to cilia axonemes was not grossly perturbed by the absence of *Fu* (data not shown). Taken together, our data suggests that Spag16L localizes to CP structures independent of Fu and perhaps helps recruit Fu to the cilium or apical surface of the cell to initiate subsequent steps of CP construction. **i**, Semi-quantitative RT-PCR showing that *Fu* transcript is upregulated during MTEC differentiation. *Fu* transcript is upregulated when long cilia containing Spag16L punctae are present, and this increase in *Fu* expression continues throughout differentiation. **j**, Semi-quantitative RT-PCR demonstrates that *Kif27* transcript is upregulated during MTEC differentiation, in a manner similar to *Fu*.

a

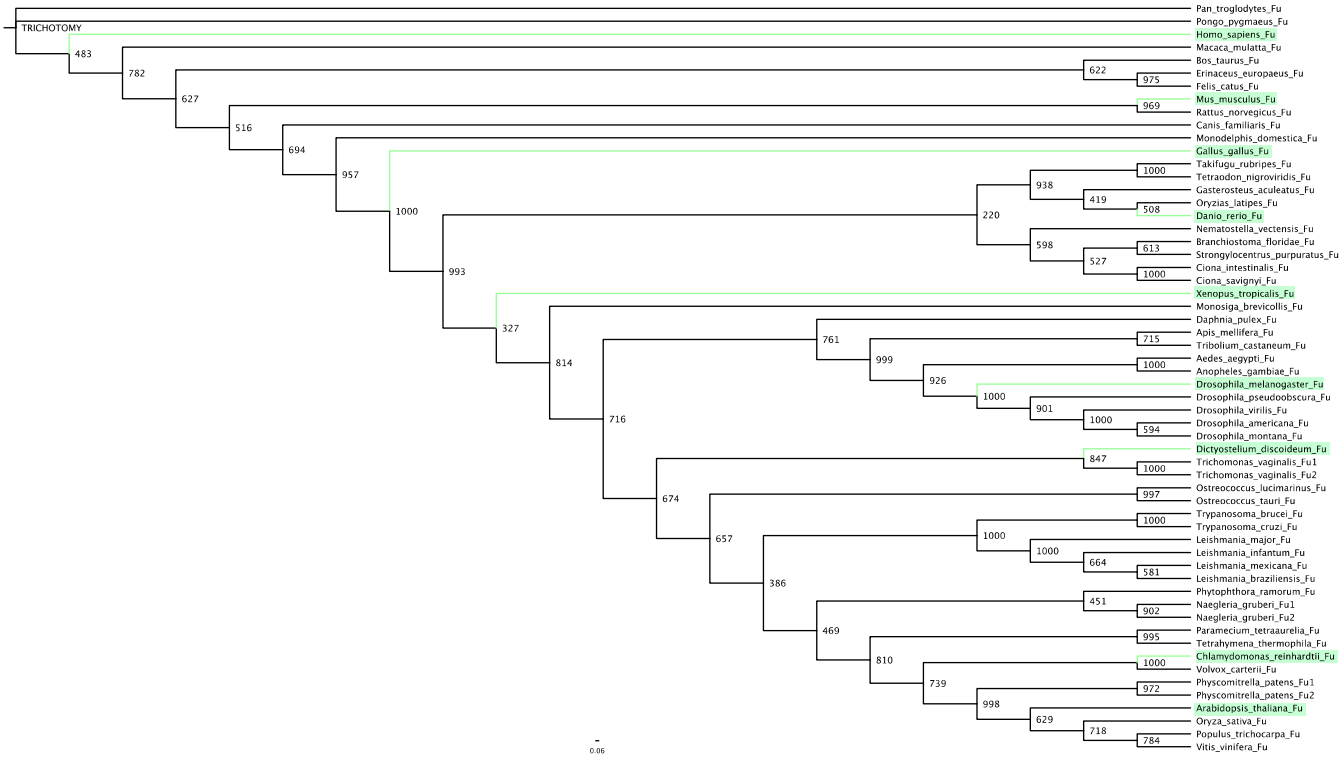

b

% ID (Sim)	H. sapiens	M. musculus	G. gallus	D. rerio	X. tropicalis	A. thaliana	D. melanogaste	C. reinhardt i	D. discoideum
H. sapiens		97 (98)	82 (90)	71 (85)	71 (84)	65 (83)	51 (69)	66 (83)	48 (74)
M. musculus	97 (98)		82 (90)	72 (86)	70 (83)	65 (83)	51 (70)	66 (83)	47 (73)
G. gallus	82 (90)	82 (90)		75 (87)	69 (84)	63 (81)	51 (70)	69 (86)	47 (74)
D. rerio	71 (85)	72 (86)	75 (87)		68 (83)	67 (83)	50 (70)	67 (85)	49 (74)
X. tropicalis	71 (84)	70 (83)	69 (84)	68 (83)		58 (77)	51 (71)	59 (81)	44 (74)
A. thaliana	65 (83)	65 (83)	63 (81)	67 (83)	58 (77)		49 (66)	78 (89)	52 (73)
D. melanogaster	51 (69)	51 (70)	51 (70)	50 (70)	51 (71)	49 (66)		51 (71)	42 (64)
C. reinhardtii	66 (83)	66 (83)	69 (86)	67 (85)	59 (81)	78 (89)	51 (71)		53 (74)
D. discoideum	48 (74)	47 (73)	47 (74)	49 (74)	44 (74)	52 (73)	42 (64)	53 (74)	

% ID (Sim)	Fu/Stk36
Akt3	34 (58)
Nek1	35 (54)
Slk	36 (56)
Ulk2	36 (55)
Ulk3	38 (58)

Supplementary Figure 8: A highly conserved Fu kinase domain is found in many eukaryotes
a, Cladogram of identified proteins containing a recognizable Fu kinase domain as assessed by BLAST against the Genbank, Ensembl v49, and JGI databases. Protein sequences of Fu kinase domains (compared against amino acids 1-289 of mouse Fu) were aligned using ClustalX and a Neighbor-Joining tree was constructed using 1000 bootstrap trials. The cladogram was constructed using FigTree v1.1.2 (Andrew Rambaut, http://tree.bio.ed.ac.uk/software/figtree). Fu kinase domains were found in metazoans, unicellular eukaryotes (many of which are flagellated, such as Chlamydomonas reinhardtii), and plant lineages. **b**, Identity/similarity matrices of Fu kinase domain sequences from highlighted species in (**a**) (top panel) and comparison of the mouse Fu kinase domain against the five most similar mouse kinases. % identity is listed first, with similarity following in parentheses. ID/sim scores were determined by pairwise BLAST. Note that the mouse Fu kinase domain has more sequence identity with predicted kinases in organisms such as Chlamydomonas and Dictyostelium than with other kinases in the mouse genome. Finally, whether utilization of the Cdc2l1 kinase implicated in Hh signaling substitutes for loss of Fu in mammalian Hh signaling remains to be further investigated[40].

Sequences used for alignments:
Genbank: Aedes aegypti: XP_001658684; Anopheles gambiae: XP_307416; Apis mellifera: XP_001122254; Arabidopsis thaliana: AAZ66047; Bos taurus: XP_585177; Canis familiaris: XP_536072; Danio rerio: AAI54436; Dictyostelium discoideum: XP_647449; Drosophila americana: AAK52244; Drosophila melanogaster: NP_477499; Drosophila montana: AAK52263; Drosophila pseudoobscura: XP_001354387; Drosophila virilis: AAF08703; Homo sapiens: AAF97028; Leishmania braziliensis: XP_001563169; Leishmania infantum: XP_001464058; Leishmania major: XP_001681788; Leishmania mexicana: CAC07966; Mus musculus Akt3: NP_035915; Mus musculus Fu: NP_778196; Mus musculus Nek1: NP_780298; Mus musculus Slk: NP_033315; Mus musculus Ulk2: NP_038909; Mus musculus Ulk3: XP_930106; Oryza sativa: NP_001066683; Paramecium tetraaurelia: XP_001423533; Rattus norvegicus: XP_217435; Strongylocentrus purpuratus: XP_001199175; Tetrahymena thermophila: XP_001029696; Tetraodon nigroviridis: CAG02878; Tribolium castaneum: XP_968708; Trichomonas vaginalis: XP_001579585, XP_001315744; Trypanosoma brucei: XP_828523; Trypanosoma cruzi: XP_806327; Vitis vinifera: CAN74245

Ensembl v49: Ciona intestinalis: translation of GENSCAN00000086241; Ciona savignyi: translation of FGENESH00000074666; Erinaceus europaeus: translation of GENSCAN_GS00000265665; Felis catus: ENSFCAG00000004156; Gallus gallus: ENSGALP00000018526; Gasterosteus aculeatus: ENSGACG00000020417; Macaca mulatta: ENSMMUP00000008885; Monodelphis domestica: ENSMODP00000019211; Oryzias latipes: translation of GENSCAN00000055611; Pan troglodytes: ENSPTRP00000022091; Pongo pygmaeus: ENSPPYP00000014729; Takifugu rubripes: Translation of GENSCAN00000027428

JGI: Branchiostoma floridae: estExt_gwp.C_740166, protein ID 280005; Chlamydomonas reinhardtii: e_gwH.30.66.1, protein ID 104702; Daphnia pulex: fgenesh1_pg.C_scaffold_99000069; protein ID: 112727; Monosiga brevicollis: fgenesh2_pg.scaffold_34000051, protein ID 29411; Naegleria gruberi: e_gw1.30.5.1, protein ID 34462; fgeneshNG_pm.scaffold_72000002, protein ID 60972; Nematostella vectensis: e_gw.384.53.1, protein ID 136852; Ostreococcus lucimarinus: e_gwEuk.15.194.1, protein ID 40725; Ostreococcus tauri: e_gw1.16.00.183.1, protein ID 21800; Physcomitrella patens: e_gw1.53.10.1, protein ID 125145; e_gw1.72.81.1, protein ID 128827; Phytophthora ramorum: fgenesh1_pg.C_scaffold_23000141, protein ID 77329; Populus trichocarpa: fgenesh4_pg.C_LG_XIX000544, protein ID 780405; Volvox carterii: e_gw1.64.130.1, protein ID 67317; Xenopus tropicalis: estExt_fgenesh1_pg.C_6450031, protein ID 459387

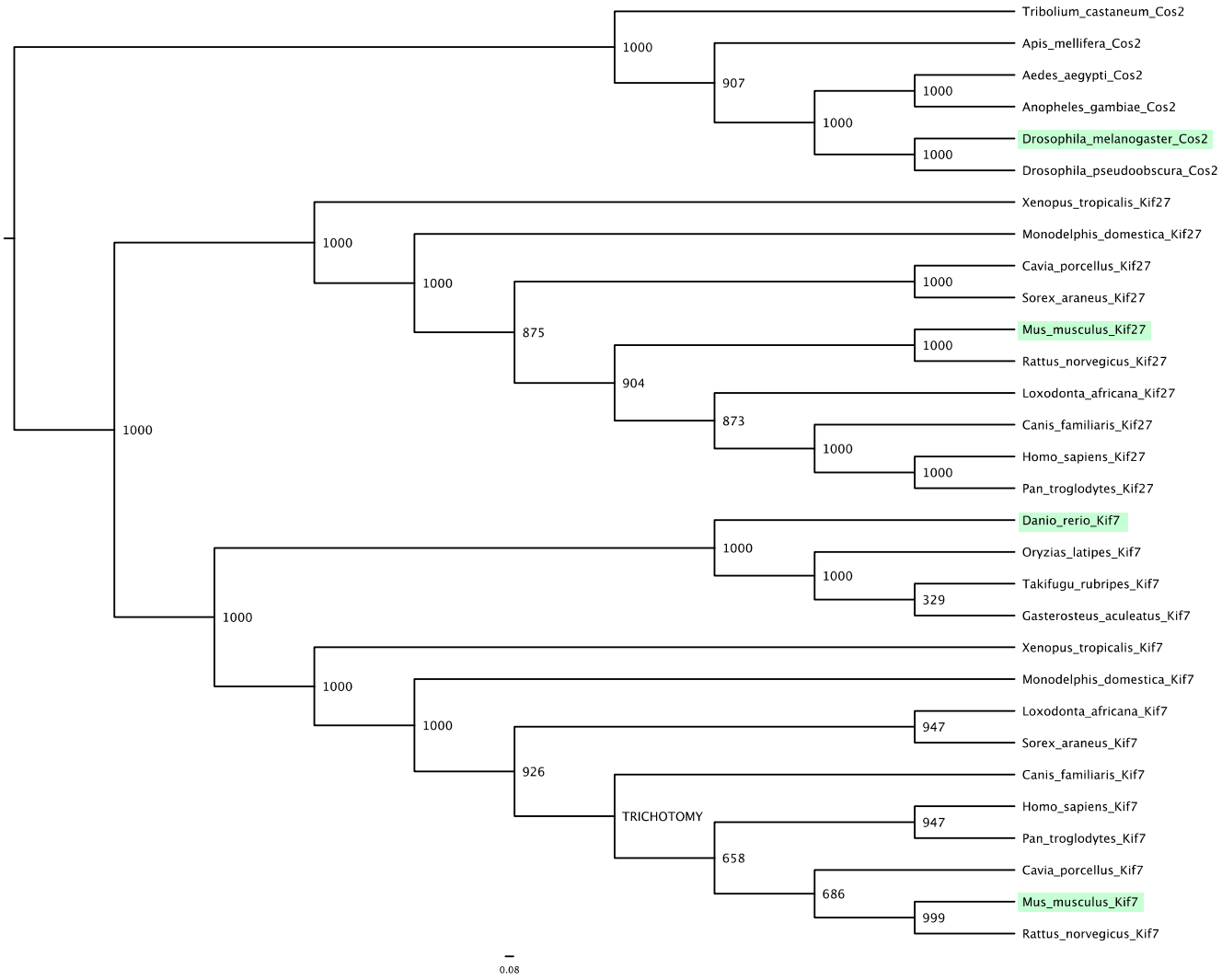

Supplementary Figure 9: Kif27 is found in mammalian lineages

Cladogram of Costal-2 (Cos2), Kif27, and Kif7 protein sequences. Full-length sequences were aligned, bootstrapped and displayed as in Supplementary Figure 8. No obvious definitive homologs to mammalian Kif27 were found in the four fish lineages examined; the closest relative to mouse Kif27 in Danio rerio, Oryzias latipes, Takifugu rubripes, and Gasterosteus aculeatus is Kif7 (data not shown). Taken together, two orders of events seem possible. First, an ancient duplication of the Cos2 ancestor resulted in the Kif7 and Kif27 genes, and the Kif27 gene was lost in the fish lineage. Second, the ancestral Kif7 gene may have undergone duplication in the tetrapod lineage, favored by the presence of both Kif7 and Kif27 in Xenopus tropicalis. Comprehensive sequence analysis of the kinesin superfamily indicates that the kinesin-4 family, of which Kif7 and Kif27 are members, has a high number of gene duplication events, which may underlie potential subfunctionalization of Kif7/Kif27 in mammals[41, 42].

Sequences used for alignments:
Genbank: Aedes aegypti Cos2: XP_001660954; Anopheles gambiae Cos2: XP_001688251; Apis mellifera Cos2: XP_624554; Danio rerio Kif7: NP_001014816; Drosophila melanogaster Cos2: NP_477092; Drosophila pseudoobscura Cos2: XP_001360209; Homo sapiens Kif7: Q2M1P5; Homo sapiens Kif27: NP_060046; Mus musculus Kif7: XP_001478724; Mus musculus Kif27: NP_780423; Rattus norvegicus Kif7: XP_218828; Rattus norvegicus Kif27: NP_932167; Tribolium castaneum Cos2: XP_973391

Ensembl v49: Canis familiaris Kif7: translation of GENSCAN00000060692; annotated peptide is ENSCAFP00000017637; Canis familiaris Kif27: ENSCAFP00000002032; Cavia porcellus Kif7: translation of GENSCAN00000188145, annotated peptide is ENSCPOP00000013857; Cavia porcellus Kif27: ENSCPOP00000002264; Gasterosteus aculeatus Kif7: ENSGACP00000021024; Loxodonta africana Kif7: translation of GENSCAN00000074353, annotated peptide is ENSLAFP00000005104; Loxodonta africana Kif27: ENSLAFP00000014808; Monodelphis domestica Kif7: translation of GENSCAN00000048146, annotated peptide is ENSMODP00000024385; Monodelphis domestica Kif27: ENSMODP00000035142; Oryzias latipes Kif7: ENSORLP00000011669; Pan troglodytes Kif7: XR_024331.1; Pan troglodytes Kif27: ENSPTRP00000035996; Sorex araneus Kif7: translation of GENSCAN00000271575, annotated peptide is ENSSARP00000010204; Sorex araneus Kif27: ENSSARP00000011952; Takifugu rubripes Kif7: ENSTRUP00000046370; Xenopus tropicalis Kif7: translation of GENSCAN00000012159, annotated peptide is ENSXETP00000038484; Xenopus tropicalis Kif27: ENSXETP00000005053

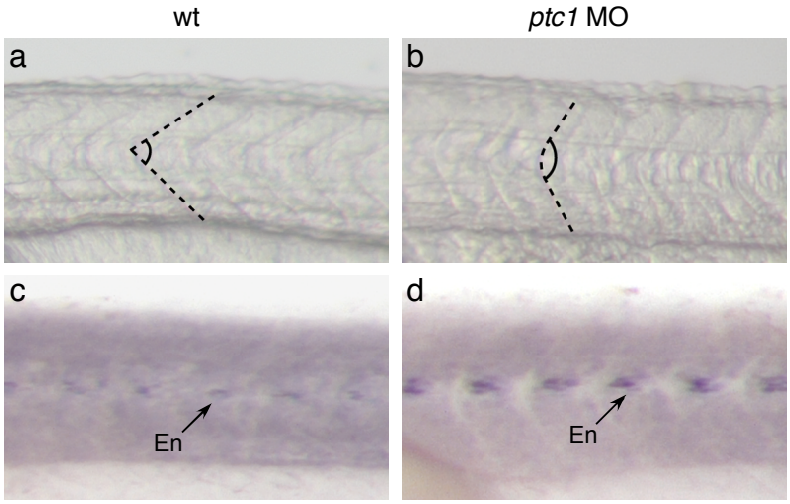

Supplementary Figure 10: Muscle differentiation is defective in *ptc1* morphants
a, **b**, Lateral view of zebrafish embryos at 24 hpf. The chevron-shaped somites in wild-type (**a**) become u-shaped in *ptc1* morphants (**b**) commonly seen in fish with disrupted Hh signaling. **c**, **d**, Whole mount immunohistochemistry against Engrailed 1 (En), which labels muscle pioneer cells in wild-type zebrafish embryos (**c**) at 24 hpf. The En-positive muscle pioneer population is expanded in *ptc1* morphants (**d**) due to up-regulation of Hh signaling through efficient knockdown of *ptc1*.

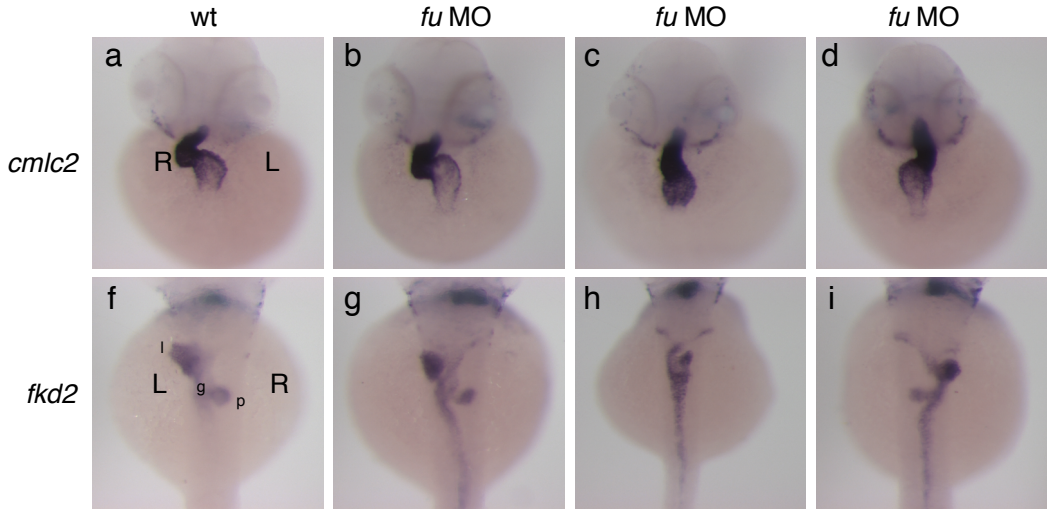

e

	#	% L	% R	% M
wt	98	94	4	2
fu MO	173	54	21	25
fu MO + mFu	80	86	10	4

j

	#	% L	% R	% M
wt	206	95	2	3
fu MO	130	70	6	24
fu MO + mFu	134	96	2	2

Supplementary Figure 11: *cmlc2* and *fkd2* expression is randomized in *fu* morphants
a-d, Whole-mount *in situ* hybridization to *cmlc2* in wt (**a**) and *fu* morphants (**b-d**) at 48 hours post fertilization (hpf). *cmlc2* expression marks the looping heart. View is ventral. **e**, Summary of cardiac laterality defects in wt, *fu* morphants, and *fu* morphants rescued with mouse *Fu*. L, atrium on the left; R, atrium on the right; M, straight heart tube. **f-i**, Whole mount *in situ* hybridization to *fkd2* in wt (**f**) and *fu* morphants (**g-i**) at 48 hpf. *fkd2* expression marks the endodermally derived gut, liver and pancreas. Medial (**h**) and inverted (**i**) expression of *fkd2* is observed in *fu* morphants. View is dorsal. l, liver; g, gut; p, pancreas. **j**, Summary of organ laterality defects in wt, *fu* morphants, and *fu* morphants rescued with mouse *Fu*. L, left; R, right; M, medial.

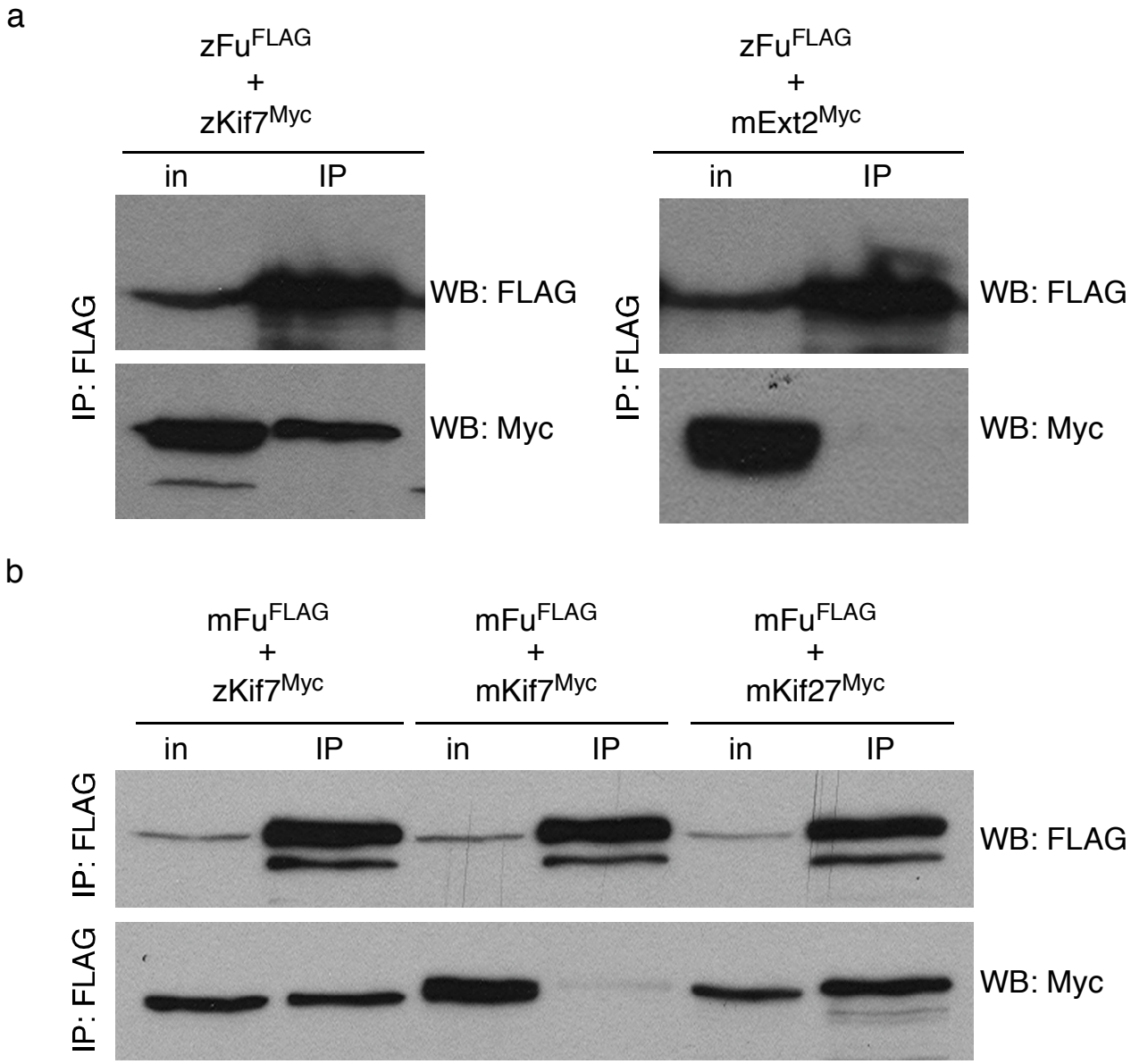

Supplementary Figure 12: Zebrafish Fu co-immunoprecipitates zebrafish Kif7
a, Western blot of immunoprecipitated zebrafish (z) Fu (epitope-tagged with four copies of FLAG) to detect physical interaction with zebrafish Kif7 (epitope-tagged with two copies of Myc) from HEK 293T lysates. WB, western blot; in, input; IP, immunoprecipitation. Zebrafish Fu interacts weakly with zebrafish Kif7, but not with an unrelated control protein (Myc-tagged mouse Ext2). Transfections, cell lysis, and immunoprecipitation with FLAG-M2 agarose were performed as described in **Full Methods**, except the concentration of NaCl used in the wash buffer was raised to 300 mM. Similar results were obtained when cell lysis and immunoprecipitation were performed in RIPA buffer (data not shown). **b**, Western blot of immunoprecipitated mouse (m) Fu (epitope-tagged with one copy of FLAG) to detect physical interaction with zebrafish Kif7 (epitope-tagged with two copies of Myc) from HEK 293T lysates. Mouse Fu co-immunoprecipitates zebrafish Kif7 and mouse Kif27, but not mouse Kif7. The interaction of mouse Fu with zebrafish Kif7 provides a mechanistic explanation for the ability of mouse *Fu* to rescue zebrafish *fu* morphants.

References

38. Chen, M. H., Li, Y. J., Kawakami, T., Xu, S. M. & Chuang, P. T. Palmitoylation is required for the production of a soluble multimeric Hedgehog protein complex and long-range signaling in vertebrates. Genes Dev 18, 641-59 (2004).

39. Gerber, A. N., Wilson, C. W., Li, Y. J. & Chuang, P. T. The hedgehog regulated oncogenes Gli1 and Gli2 block myoblast differentiation by inhibiting MyoD-mediated transcriptional activation. Oncogene 26, 1122-36 (2007).

40. Evangelista, M. et al. Kinome siRNA screen identifies regulators of ciliogenesis and hedgehog signal transduction. Sci Signal 1, ra7 (2008).

41. Miki, H., Okada, Y. & Hirokawa, N. Analysis of the kinesin superfamily: insights into structure and function. Trends Cell Biol 15, 467-76 (2005).

42. Lynch, M. & Conery, J. S. The evolutionary fate and consequences of duplicate genes. Science 290, 1151-5 (2000).